Component Level Uncertainty Quantification of Thickness Estimations Computed from Full-Field Ultrasonic Inspection

CLARA S. BENDER, ERICA M. JACOBSON, ERIC B. FLYNN and ADAM J. WACHTOR

ABSTRACT

This work performs a case study on the error and uncertainty of thickness estimations derived from acoustic steady-state excitation spatial spectroscopy (ASSESS) – a full-field ultrasonic inspection technique that can be utilized for structural health monitoring applications. Thickness estimation was performed using a 40 kHz excitation frequency on 0.2 m x 0.2 m steel plates ranging in thickness between 1.55 mm and 19.14 mm. The experimental thickness estimation results were compared to corresponding analytical results and thickness errors resulting from experimental uncertainties were investigated.

INTRODUCTION

Acoustic steady-state excitation spatial spectroscopy (ASSESS) works by exciting a structure at a constant frequency and collecting its surface vibrational response using a scanning laser Doppler vibrometer (LDV). A LiDAR simultaneously collects surface geometry to allow perspective correction of the wavefield measured by the LDV. The resulting wavefield of the structure's response can be used to derive localized thickness estimates and identify regions of corrosion or other damage through wavenumber evaluation.

Wavenumber, the inverse of wavelength, has been identified as a time-invariant way to characterize defects within a structure – allowing for the use of steady-state excitation in ultrasonic nondestructive evaluation, which is orders of magnitude faster and has greater signal-to-noise ratio than transient excitation methods [1]. Researchers have since applied wavenumber evaluation methods to detect and quantify delamination in composites and thickness loss in aluminum [1-5]. The accuracy of the wavenumber method in damage detection and thickness estimation is dependent on the excitation frequency and the modes excited, and their optimization has been studied by [6] and [7].

The errors and uncertainties associated with the data collection and processing for thickness estimation using the ASSESS technique have not yet been fully

Los Alamos National Laboratory, 4200 W. Jemez Rd, Los Alamos, New Mexico 87545, U.S.A.

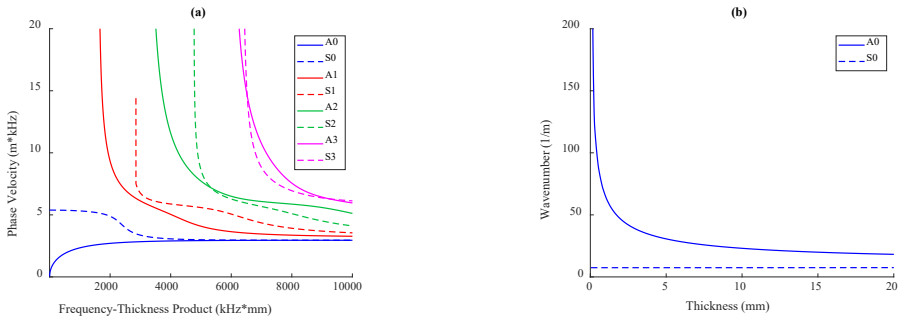

Figure 1: a) 1020 steel acoustic dispersion curves. b) Steel 1020 dispersion curves at 40kHz.

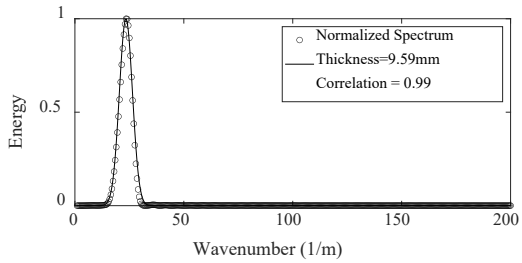

Figure 2: 1D wavenumber spectrum for a pixel from 9.64 mm St plate with template match.

characterized, which is necessary for the broader industry adoption. This paper identifies possible sources of error for consideration when employing the ASSESS thickness estimation system through a case study of eight steel plates of thicknesses varying between 1.55 mm and 19.14 mm excited at 40 kHz.

METHODS

The expected wavenumber spectrum for a given thickness is found using Lamb wave theory, which assumes an infinite isotropic homogeneous plate. Lamb wave propagation through a material is described by dispersion curves, which link frequency-thickness products to phase velocity (fig. 1a). The S0 and A0 wave modes are excited at every frequency-thickness product, and as frequency-thickness product increases, more modes are excited. Given a constant excitation frequency, dispersion curves can be calculated that connect the local wavenumber estimated from the vibrational response to thickness (fig. 1b). The thickness estimation algorithm works by estimating the local wavenumber spectrum centered at each data pixel and then finding the best thickness match with the acoustic dispersion curve.

A thickness estimation template is made from the dispersion curve by forming a Gaussian over the wavenumber values using a bandwidth that best matches the bandwidth found in the local wavenumber spectra (fig. 2). The Pearson's correlation coefficient is found between each localized wavenumber spectrum and the spectrum of each thickness candidate. The thickness associated with the maximum correlation becomes the estimated thickness.

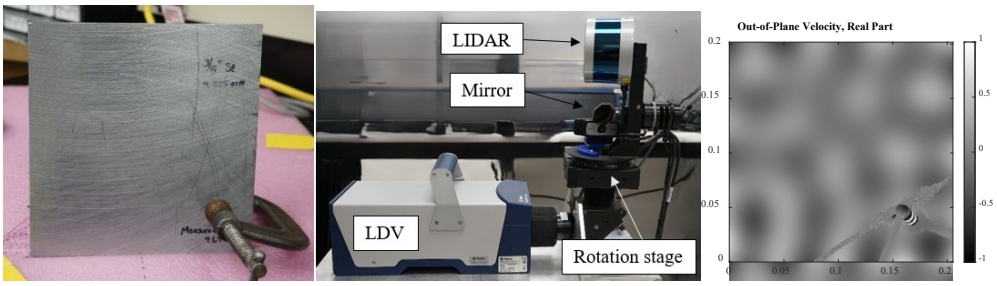

Figure 3: (left) Steel plate with a transducer clamp that was also used to hold the plate up and close to perpendicular to the LDV. (middle) Laser of the LDV was directed via a galvanometer mirror and a horizontal rotation stage. LIDAR is also mounted on rotation stage and aligned with LDV laser. (right) Example of a wavefield response map from the ASSESS measurement system.

Experimental Data Collection

Eight $(0.2\text{ m})^2$ ground, low-carbon steel plates with thicknesses of 1.55, 2.41, 3.25, 4.05, 6.49, 9.64, 12.70, and 19.14 mm were individually excited at a constant frequency of 40 kHz via a transducer clamped to the lower righthand corner. The surface vibration response was measured by a scanning LDV located approximately 2 m away with a scan speed of 8 pixels/ms and a pixel resolution of $(0.56\text{ mm})^2$, resulting in a 2D complex wavefield response map. Perspective correction was performed on the wavefield using geometric data collected by a LiDAR, such that the final analysis image represented the out-of-plane velocity response (fig. 3).

Analytical Data Generation

Analytical velocity data was generated for plates with the same thicknesses, pixel resolution, and excitation frequency as the experimental plate measurements. The analytical wavefield map was calculated by finding the expected wavenumber response for each plate thickness from the dispersion curve for 1020 steel and adding together waves of that wavenumber from one or multiple point sources (7).

The wave modes included in the analytical model were determined by estimating mode contribution seen in the experimental data. Mode contribution estimation was performed by applying a Kaiser window with $\beta = 4$ to the experimental velocity data, computing the 2D Fourier transform, and then taking the radial average to determine the 1D wavenumber spectrum. Each peak in the 1D wavenumber spectrum was identified with a wave mode, the magnitude of which indicated the presence of that mode in the out-of-plane velocity response data. For all eight plates excited at 40 kHz, the S0 mode made up less than 5% of the waveform and the A0 mode made up of the rest of the waveform. Therefore, only the analytical simulations were chosen to only include the A0 mode for simplicity. Analytical models for an infinite plate (non-reflecting) and a finite plate for each of the thicknesses were created (fig. 4). The source placement for the finite plate was chosen to create a waveform that emulated that of an experimental measurement.

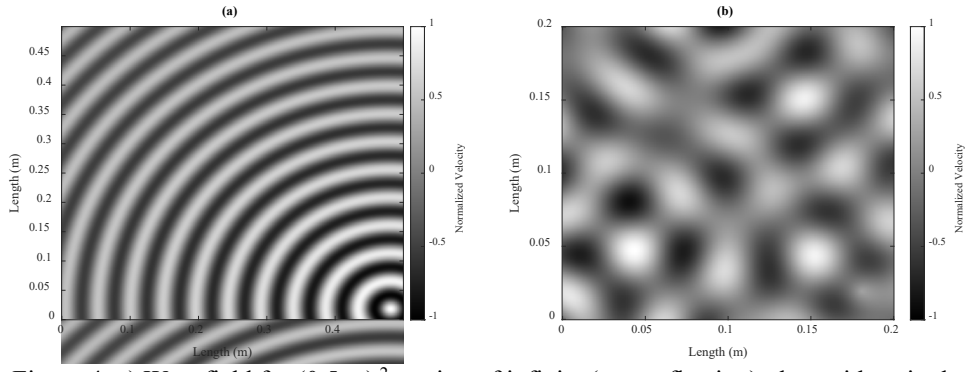

Figure 4: a) Wavefield for $(0.5\text{ m})^2$ section of infinite (non-reflecting) plate with a single point source at [0.48 m, 0.02 m]. b) Wavefield for $(0.2\text{ m})^2$ finite plate and point sources located at [0.18 m, 0.02 m], [0.1 m, -0.01 m], [-0.02 m, -0.01 m], [-0.02 m, 0.1 m], [-0.5 m, 0.7 m], [0.1 m, 0.22 m], [0.2 m, 0.21 m], and [0.21 m, 0.1 m]. Pixel resolution of $(0.56\text{ mm})^2$.

Localized Thickness Estimation

Localized thickness estimation was performed on both the experimental and analytical data sets by passing the 2D wavenumber spectrum data through a series of Gabor filters with a standard deviation of 0.002 and central wavenumbers varying from 1-200 m^{-1} in increments of 0.5 m^{-1}. The inverse Fourier transform of the filtered wavenumber spectrum resulted in the monogenic signal at each of the central wavenumbers, square of which represents the energy associated with that wavenumber for each pixel. The local energies at each central wavenumber were combined into a 1D wavenumber spectrum for each pixel and then matched to thickness using the thickness matching template for 1020 Steel excited at 40 kHz containing only the A0 mode.

Error and Uncertainty Quantification

Thickness estimation was performed on the analytical and experimental data, and the mean, μ, and standard deviation, σ, from the central $(0.1\text{ m})^2$ square region of the plate were calculated to reduce the effects of boundary conditions. The results for the analytical infinite plate simulations served to validate the thickness estimation code. The processing results for the analytical finite plates served to quantify the error due to the Fourier transform being applied to a finite domain. The remaining experimental error source was investigated by assessing the collection variability, LiDAR measurement uncertainty used for perspective correction, and effects of material properties when computing the dispersion curves.

The variability of the collection system was investigated by comparing thickness mean and standard deviation of the central $(0.1\text{ m})^2$ square for a 0.2 m x 0.2 m, 9.64 mm thick steel plate excited at a frequency of 40 kHz over six trials performed in succession.

The perspective correction uncertainty was calculated assuming an uncertainty of $\pm$3cm, as given by the LiDAR manufacturer, in the out-of-plane direction of the plate. The resulting pixel size error was related to A0 wavenumber error, then to thickness estimation error via the 1020 Steel dispersion curve.

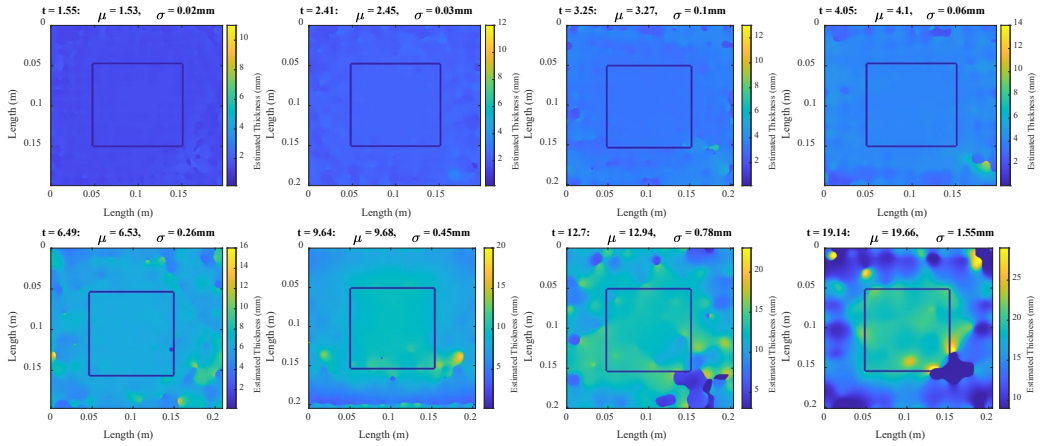

Figure 5: Experimental thickness estimation results for $(0.2\ \text{m})^2$ steel plates excited at 40kHz. Mean and standard deviation were calculated from outlined square.

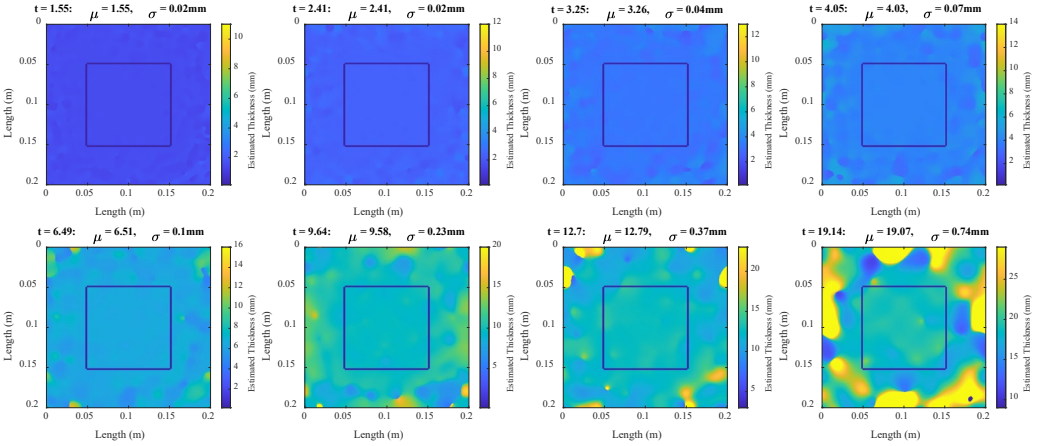

Figure 6: Analytical thickness estimation results for $(0.2\ \text{m})^2$ steel plates excited at 40kHz. Mean and standard deviation were calculated from the outlined square.

The experimental steel plates used for this analysis were ground, low-carbon steel, in the range of 1006 steel to 1026 steel. To determine the sensitivity of the thickness estimation to using dispersion curves of varying steel alloys in the analysis, the theoretical thickness error was determined for a 1006 steel, 1008 steel, and 1026 steel plate if a 1020 steel was incorrectly assumed and used for the computation of the dispersion curve.

RESULTS

Thickness Estimation for Experimental and Analytical Plates

For the thickness estimation of the analytical infinite plate, the largest mean error was 0.008 mm and the largest standard deviation was 0.004 mm.

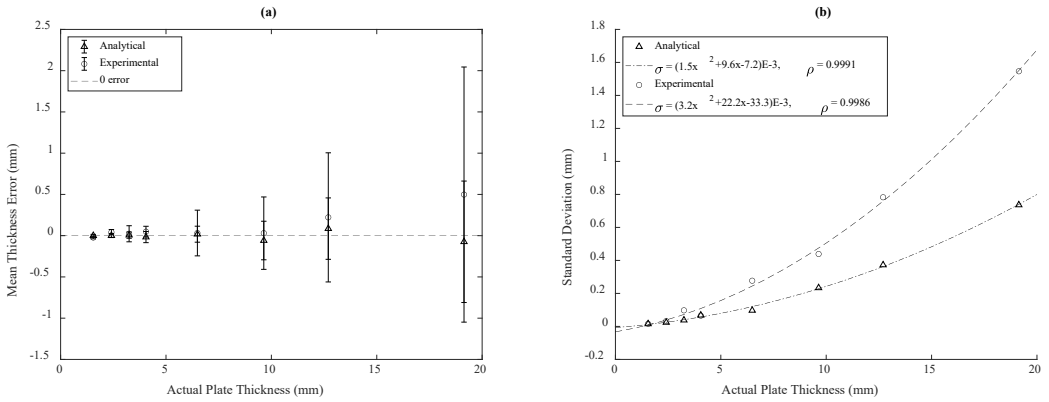

Figure 7: a) Mean thickness error for the central $(0.1\ \text{m})^2$ square of thickness estimation with error bars. b) Thickness standard deviation for central $(0.1\ \text{m})^2$ square of thickness estimation.

The localized thickness estimation results from the experimental and analytical finite plates had greater accuracy and uniformity for lower thicknesses. Edge effects became more prevalent at higher plate thicknesses and started to influence the region for which statistics were determined around a thickness of 10 mm (figs. 5-6).

For both experimental and analytical finite plate data, the true thicknesses were within one standard deviation of the mean estimate (fig. 7a). The analytical mean error magnitude centered around zero with maximum of 0.07 mm. The experimental mean error was roughly uniform and less than 0.1mm for thicknesses below 10 mm and then increased to 0.2 mm at 12.70 mm and 0.5 mm at 19.14 mm. The thickness standard deviation increased quadratically with the true plate thickness for the experimental and analytical data, demonstrating algorithm limitations for finite geometries. The experimental data had a faster growth rate than the analytical data (fig. 7b) that may be explained by other sources of error explored in the following sections.

Collection Variability and LIDAR Perspective Correction Error

Between six successive experimental trials of the 9.64 mm steel plate excited at 40kHz, the thickness mean varied from 9.61 to 9.67 mm, and the standard deviation varied from 0.39 to 0.44 mm.

The potential thickness error due to the ± 3cm uncertainty applied to the out-of-plane direction of the plate was greater than the experimental mean error for all thicknesses and grew with increasing thickness (fig. 9).

Dispersion Curve Error

The A0 mode of the 1020 steel dispersion curve had a lower wavenumber than the 1006, 1008, and 1026 steel dispersion curves for all thicknesses at 40kHz. The magnitude of the wavenumber difference decreased as plate thickness increased until it approached an asymptotic magnitude for the range of thicknesses tested (fig. 9a). The underestimation in the wavenumber regime led to overestimation in the thickness regime (fig. 10b). Because of the shape of the dispersion curves, the thickness

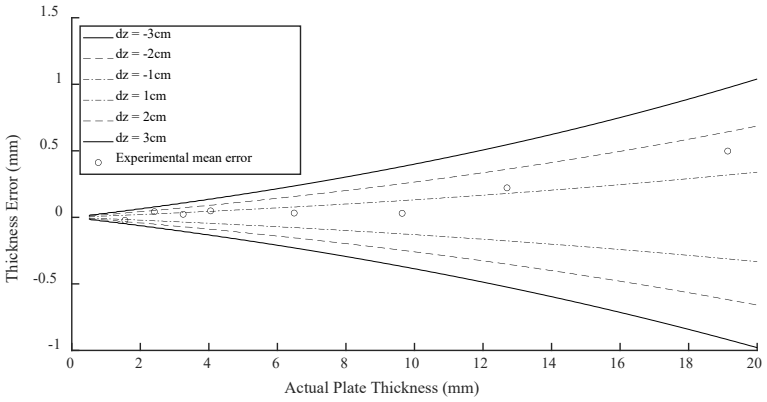

Figure 8: LiDAR thickness error at a plate distance of 2 meters for an uncertainty of 1, 2, and 3 cm, plotted with experimental mean error.

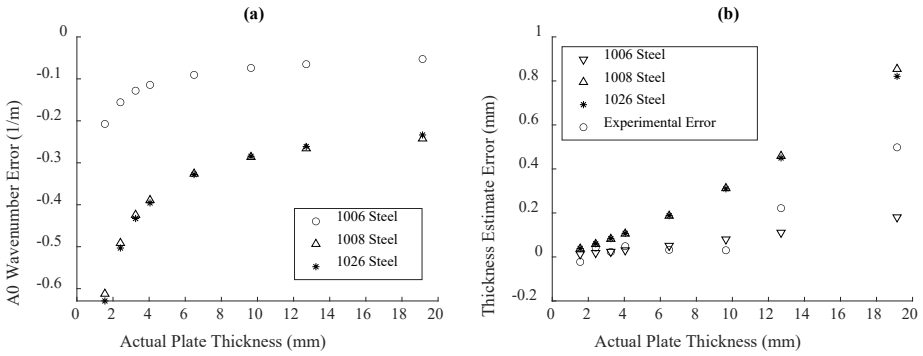

Figure 9: a) Theoretical wavenumber error from analyzing a 1006, 1008, and 1026 steel plate with a 1020 steel dispersion curve. b) Theoretical thickness error from analyzing a 1006, 1008, and 1026 steel plate with a 1020 steel dispersion curve, plotted with experimental error.

estimation error increased with thickness. For each of the plate thicknesses, the experimental mean error did not exceed the largest possible dispersion curve error.

CONCLUSION

The thickness analysis of the analytical infinite plate validated the thickness estimation processing using the Lamb wave assumption. Thickness estimation of the analytical finite plates in comparison with the experimental plates demonstrated a strong correlation between thickness estimation uncertainty and the limitations of the algorithm for a finite domain, as witnessed by both the experimental and analytical standard deviations growing quadratically with thickness.

The investigation of potential errors caused by steel alloy dispersion curve inaccuracy and LIDAR inaccuracy revealed that these were significant in comparison to the measured experimental mean error, while collection variability was not. Further work would be needed to identify the source of the additional error that was seen in the experimental data over that determined from the analytical simulations. Dispersion curve inaccuracy could be mitigated through direct measurement of modulus of elasticity, Poisson's ratio, and density of a sample material and using

those specific to the material for calculating the dispersion curve, rather than taking a representative material from the known class. The LiDAR error could be directly measured by comparing the plate distance found by the LiDAR to a measurement using a tape measure or other range finding device. The fact that the mean error was significantly greater for the 12.70 and 19.14mm plates suggests more advanced algorithms may be needed to compensate for the decreased slope of the dispersion curves for larger thicknesses.

This work lays an essential foundation for identifying limitations and quantifying uncertainties for the ASSESS measurement system for thickness analysis – an imperative step for adoption of this inspection technique within highly standardized industries.

REFERENCES

1. E. B. Flynn, S. Y. Chong, G. J. Jarmer, and J. R. Lee, "Structural imaging through local wavenumber estimation of guided waves," *NDT&E International*, vol. 59, pp. 1–10, 2013, doi: 10.1016/j.ndteint.2013.04.003.
2. J. Y. Jeon, S. Gang, G. Park, E. Flynn, T. Kang, and S. Woo Han, "Damage detection on composite structures with standing wave excitation and wavenumber analysis," *Advanced Composite Materials*, vol. 26, pp. 53–65, May 2017, doi: 10.1080/09243046.2017.1313577.
3. J. Spytek, L. Pieczonka, T. Stepinski, and L. Ambrozinski, "Mean local frequency-wavenumber estimation through synthetic time-reversal of diffuse Lamb waves," *Mechanical Systems and Signal Processing*, vol. 156 (107712), pp. 1-11.
4. J. Spytek and L. Pieczonka, "Local wavenumber imaging in anisotropic structures," *Mechanical Systems and Signal Processing*, vol. 224 (112102), pp. 1-14.
5. S. Kang, E. B. Flynn, J. Y. Jeon, and G. Park, "Damage detection on thin walled structures with single frequency excitation and wavenumber filtering," *8th EWSHM*, Bilbao, Spain, 2016, vol. 4, pp. 3051-3060.
6. T. Kang, S. Moon, S. Han, J. Y. Jeon, and G. Park, "Measurement of shallow defects in metal plates using inter-digital transducer-based laser-scanning vibrometer," *NDT&E International*, vol. 102, pp. 26-34, 2019, doi: 10.1016/j.ndteint.2018.11.004.
7. N. D. Stull, M. Mascarenas, and E. B. Flynn, "On performance limits in estimating thickness of a plate-like structure from a full-field single-tone response Lamb wave measurement," *11th IWSHM*, Stanford, CA, 2017.